Bulletin of the New Zealand Society for Earthquake Engineering, Vol. 48, No. 4, December 2015

PERFORMANCE EVALUATION OF CWH BASE ISOLATED BUILDING DURING TWO MAJOR EARTHQUAKES IN CHRISTCHURCH

Cong Zhou[1], J. Geoffrey Chase[2], Geoffrey W. Rodgers[3], Adam Kuang[4], Stefanie Gutschmidt[5] and Chao Xu[6]

(Submitted *July 2015*; Reviewed *October 2015*; Accepted *November 2015*)

ABSTRACT

The seismic performance and parameter identification of the base isolated Christchurch Women's Hospital (CWH) building are investigated using the recorded seismic accelerations during the two large earthquakes in Christchurch. A four degrees of freedom shear model is applied to characterize the dynamic behaviour of the CWH building during these earthquakes. A modified Gauss-Newton method is employed to identify the equivalent stiffness and Rayleigh damping coefficients of the building. The identification method is first validated using a simulated example structure and finally applied to the CWH building using recorded measurements from the M_w 6.0 and M_w 5.8 Christchurch earthquakes on December 23, 2011. The estimated response and recorded response for both earthquakes are compared with the cross correlation coefficients and the mean absolute percentage errors reported. The results indicate that the dynamic behaviour of the superstructure and base isolator was essentially within elastic range and the proposed shear linear model is sufficient for the prediction of the structural response of the CWH Hospital during these events.

INTRODUCTION

The isolation of structures from the ground motion is an effective way to protect the structure from damage in a strong earthquake. The basic concept of base isolation is to provide a low lateral stiffness between the structure and the foundation to lengthen the natural period of the building from its fixed-base value and the dominant periods of the seismic ground motion. Thus, the transmission of earthquake motion and force to the superstructure of the isolated building can be significantly reduced.

Successful field performance of base-isolated buildings was first recorded and validated in the University of Southern California (USC) Hospital building during the 1994 Northridge earthquake. Due to the lead rubber bearings (LRBs) isolation system, peak roof accelerations were reduced to 50% of the foundation acceleration, and the peak drift of the superstructure was less than 30% of the code specification [1].

The measured response of two high damping rubber bearing isolated buildings in Miyagi and Chiba, Japan were investigated during the 2011 Tohoku earthquake [2]. The study confirmed acceleration reductions in both buildings, and the maximum accelerations at the floor above the isolated layer were 41-83% of those in the basement. The strong motion seismic records of Fukushima Dai-Ichi Nuclear Power Plant were also reported in the Great East Japan Earthquake in 2011 [3]. This base-isolated structure performed well in horizontal motion with the response reduced by 30% from the basement pit.

The Christchurch Women's Hospital (CWH) building was opened in 2005 and is the only base-isolated structure in the South Island of New Zealand. The base isolation system of the CWH building consists of 41 LRBs and four pot bearings founded on a concrete raft. The design specifications of the LRBs and pot bearings are listed in Tables 1 and 2, respectively [4].

Table 1: Design parameters for LRBs bearings.

Designation	Total design displacement (mm)	Total maximum displacement (mm)	Compression stiffness (kN/mm)	Design shear force at total design displacement (kN)	Average (dead load(DL)+serviceability live load (SLL)) (kN)	Maximum (DL+ live load (LL)) (kN)
LRBs	265	420	1794	740	3495	4417

Table 2: Design parameters for pot bearings.

Designation	Average (DL+ SLL) (kN)	Maximum (DL+ LL) (kN)	Maximum motion (mm)	Maximum rotation (rad)	Maximum dynamic friction coefficient (dry)
Pot Bearings	4986	5768	+/-420	0.006	0.12

[1] *Corresponding Author, PhD Candidate, University of Canterbury, Christchurch, cong.zhou@pg.canterbury.ac.nz.*
[2] *Distinguished Professor, University of Canterbury, Christchurch (Member)*
[3] *Senior Lecturer, University of Canterbury, Christchurch (Member)*
[4] *PhD Candidate, Massachusetts Institute of Technology, Cambridge*
[5] *Senior Lecturer, University of Canterbury, Christchurch*
[6] *Associate Professor, Northwestern Polytechnical University, Xian*

The superstructure has eight levels, including four V-bracing levels, three levels without V-bracing, and the top level containing service equipment and four water tanks. A network of instruments was installed in September 2011 after a magnitude 6.3 (M_w6.3) earthquake on February 22nd 2011 in Christchurch that caused severe damage to the city business district and resulted in the loss of 185 lives. The monitoring sensors recorded the acceleration of the foundation, the first level just above the isolation layer and the eighth level of the building during two major earthquakes (M_w 5.8 at 1:58pm and M_w 6.0 at 3:18pm local time) on December 23rd 2011. These recordings provide a unique opportunity to identify a structure for two, similarly sized large events occurring within a few hours on an essentially unchanged structure.

A number of researchers have investigated the parameter identification methods for base-isolated buildings using different system models. Stewart *et al*. [5] identified the structural modal parameters of four isolated buildings using an equivalent time-varying linear model, based on the assumption of the superstructure as an SDOF system and the isolation system with time-varying effective stiffness, to characterize the isolation performance during the earthquake. Furukawa *et al*. [6] proposed a least-squares output-error minimization method to identify a base-isolated building affected by the 1995 Hyogoken-Nambu earthquake in Japan. The superstructure was modelled as a rigid body and the isolation system was identified based on three different models: a linear equivalent model, a bilinear model and a tri-linear model. Results showed that the model parameters can be reasonably estimated and the tri-linear model best fit the recorded response time histories. Huang *et al*. [7] developed an iterative trial-and-error optimization procedure, based on a simplified bilinear model for the base isolation system and a multi-story linear model for the superstructure. They identified the structural parameters of a base-isolated building using a Masing criterion to transform a multi-valued hysteretic restoring force function into a single-valued function so that ordinary optimization methods can be applied. Xu *et al*. [8] recently proposed a two-step regression analysis procedure to identify the physical parameters of a base-isolated structure. A bilinear model was chosen for modelling the base isolator and the superstructure was assumed as a single-degree-of-freedom system. The hysteresis loops were divided into different half-cycles according to zero velocity points and multiple linear regression was applied to all half-cycles to yield equivalent linear system stiffness and damping.

For all these system identification methods, a key element is the choice of proper models for the base isolation system and superstructure. The choice is primarily based on the actual or expected response of the building and isolators, and is critical for accurate identification. Since the isolated building should be quite rigid in comparison to the isolation system, a superstructure is frequently assumed to be a lumped mass that reduces the computational efforts significantly [9]. Otherwise, a multi-story linear model is considered for the superstructure [10]. For the base isolation system, a nonlinear hysteretic model [11] is widely used to characterize the nonlinear force-deformation behaviour of the LRB experiencing the inelastic seismic response expected by design [1, 12, 13]. However, the properties of LRB can be modelled using a spring equivalent linear horizontal stiffness in the case that the ground motion is not very large or the base isolation system has no yielding under the ground shaking [14]. Hence, the isolation layer response may vary from the expected performance or have a range of behaviours, and thus have a significant, negative impact on the identified model's accuracy.

In this study, the seismic response of the basement and superstructure of the CWH was first analysed to obtain a four degrees of freedom shear type model for the base-isolated building. A modified Gauss-Newton method was then employed to identify the structural parameters of the proposed model and further validated using a simulated structure. The real seismic data are finally used for parameter identification to evaluate the seismic performance of the building during the two earthquakes in Christchurch.

MODEL OF ISOLATED CWH BUILDING

Figure 1 shows the accelerations for the foundation, first and top levels during the M_w6.0 and M_w5.8 earthquake events, where Figure 2 shows the locations of these measurements. Both the magnitude and phase of the recorded accelerations are different for the first and top levels during these two events. Therefore, the superstructure of the base isolated hospital building does not approximate a rigid body as might be expected of a base-isolated structure. In addition, the peak accelerations of the first and top levels were not reduced compared to the foundation, which indicates the base isolation system was still within the stiffer linear range and did not lead to the period separation of the ground shaking and the building during these two events. Thus, a multi-degree-of-freedom linear shear type model is used for parameter identification.

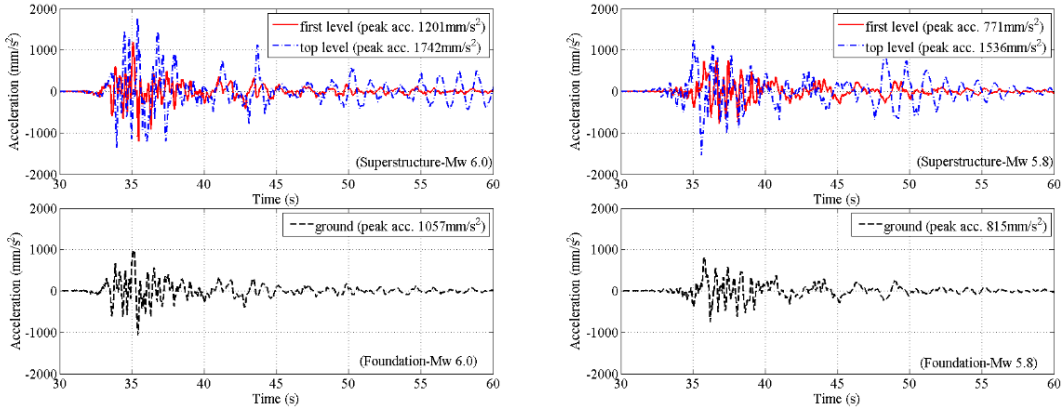

(a) (b)

Figure 1: Comparison of time histories of accelerations for the foundation, first and top floors: (a) M_w 6.0 earthquake; (b) M_w 5.8 earthquake.

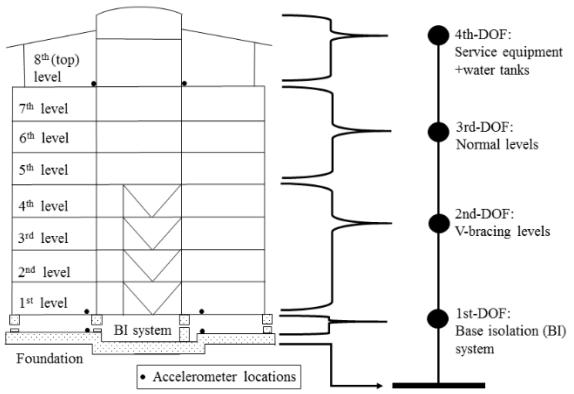

(a) (b)

Figure 2: The base isolated CWH building: (a) elevation view showing the sensor locations; (b) 4-DOF shear type model.

In particular, the base isolated hospital building is modelled as a four degrees of freedom (DOF) system in Figure 2, with the first DOF representing the base isolation system, the second DOF representing the lower four levels with V-bracing, the third DOF representing the three levels without V-bracing, and the fourth DOF containing the top level with service equipment and water tanks. These DOFs separate structural regions with known, significantly different distributions of stiffness and/or mass. The accelerations for the first and fourth DOFs, as well as the ground motion inputs in the basement, were recorded. To identify the equivalent stiffness and Rayleigh damping for the hospital building, the response for the second and third DOFs are estimated using the recorded response and model, and a modified Gauss-Newton method is employed to identify the parameters of the system.

IDENTIFICATION METHOD

The equation of motion for the based-isolated building subject to seismic excitation is defined as:

$$\mathbf{M}\ddot{x}+\mathbf{C}\dot{x}+\mathbf{K_T}x=-\mathbf{M}\mathbf{I}\ddot{x}_g \tag{1}$$

where $x=[x_1\ x_2\ x_3\ x_4]^{\mathrm{T}}$, and the mass, stiffness and estimated Rayleigh damping matrix are defined as:

$$\mathbf{M}=\begin{bmatrix} m_1 & 0 & 0 & 0 \\ 0 & m_2 & 0 & 0 \\ 0 & 0 & m_3 & 0 \\ 0 & 0 & 0 & m_4 \end{bmatrix} \tag{2}$$

$$\mathbf{K_T}=\begin{bmatrix} K_1+K_2 & -K_2 & 0 & 0 \\ -K_2 & K_2+K_3 & K_3 & 0 \\ 0 & -K_3 & K_3+K_4 & -K_4 \\ 0 & 0 & -K_4 & K_4 \end{bmatrix} \tag{3}$$

$$\mathbf{C}=a_0\mathbf{M}+a_1\mathbf{K_T}=\begin{bmatrix} C_{11} & -C_{12} & 0 & 0 \\ -C_{21} & C_{22} & -C_{23} & 0 \\ 0 & -C_{32} & C_{33} & -C_{34} \\ 0 & 0 & -C_{43} & C_{44} \end{bmatrix} \tag{4}$$

where the elements in the Rayleigh damping matrix C_{ij} are defined as:

$$\begin{aligned} C_{11}&=a_0m_1+a_1(K_1+K_2)\\ C_{22}&=a_0m_2+a_1(K_2+K_3)\\ C_{33}&=a_0m_3+a_1(K_3+K_4)\\ C_{44}&=a_0m_4+a_1K_4\\ C_{12}&=C_{21}=a_1K_2\\ C_{23}&=C_{32}=a_1K_3\\ C_{34}&=C_{43}=a_1K_4 \end{aligned} \tag{5}$$

Using Equations (1)-(4), the equation of motion for the first and fourth DOF are:

$$m_1\ddot{x}_1+C_{11}\dot{x}_1-C_{12}\dot{x}_2+(K_1+K_2)x_1-K_2x_2=-m_1\ddot{x}_g \tag{6}$$

$$m_4\ddot{x}_4-C_{43}\dot{x}_3+C_{44}\dot{x}_4-K_4x_3+K_4x_4=-m_4\ddot{x}_g \tag{7}$$

where the accelerations were measured, the velocity and displacement of x_1 and x_4 can be obtained by direct integration after band pass filtering, and K_{ij} and C_{ij} are to be identified. Equations (6) and (7) can thus be rewritten in terms of unknowns x_2 and x_3:

$$\dot{x}_2+P_1(K_2,C_{12})x_2=Q_1(K_1,K_2,C_{11},C_{12},t) \tag{8}$$

$$\dot{x}_3+P_2(K_4,C_{43})x_3=Q_2(K_4,C_{43},C_{44},t) \tag{9}$$

where:

$$P_1=\frac{K_2}{C_{12}} \tag{10}$$

$$Q_1=\frac{m_1\ddot{x}_1+C_{11}\dot{x}_1+(K_1+K_2)x_1+m_1\ddot{x}_g}{C_{12}} \tag{11}$$

$$P_2(K_2,C_{12})=\frac{K_4}{C_{43}} \tag{12}$$

$$Q_2=\frac{m_4\ddot{x}_4+C_{44}\dot{x}_4+K_4x_4+m_4\ddot{x}_g}{C_{43}} \tag{13}$$

The general solutions for Equations (8) and (9) are obtained:

$$\begin{aligned} x_2(t)&=A_ie^{-\int P_1(K_2,C_{12})dt}\\ &+e^{-\int P_1(K_2,C_{12})dt}\int Q_1(K_1,K_2,C_{11},C_{12},t)e^{\int P_1(K_2,C_{12})dt}dt \end{aligned} \tag{14}$$

$$x_3(t) = B_i e^{-\int P_2(K_4,C_{43})dt} + e^{-\int P_2(K_4,C_{43})dt}\int Q_2(K_4,C_{43},C_{44},t)e^{\int P_2(K_4,C_{43})dt}dt) \quad (15)$$

For each time step $h=t_i-t_{i-1}$, the free terms Q_1 and Q_2 in Equations (11) and (13) can be written as a moving average for $t_{i-1}\le t\le t_i$:

$$Q_{1i} = \frac{Q_1(K_1,K_2,C_{11},C_{12},t_{i-1}) + Q_1(K_1,K_2,C_{11},C_{12},t_i)}{2} \quad (16)$$

$$Q_{2i} = \frac{Q_2(K_4,C_{43},C_{44},t_{i-1}) + Q_2(K_4,C_{43},C_{44},t_i)}{2} \quad (17)$$

Substituting Equations (16) and (17) into Equations (14) and (15), respectively:

$$x_2(t) = e^{-(t-t_{i-1})/a_1}(A_i + a_1 Q_{1i} e^{(t-t_{i-1})/a_1}) \quad (18)$$

$$x_3(t) = e^{-(t-t_{i-1})/a_1}(B_i + a_1 Q_{2i} e^{(t-t_{i-1})/a_1}) \quad (19)$$

where A_i and B_i are constants determined by initial condition at $t=t_{i-1}$. If $x_2(t_{i-1})$ and $x_3(t_{i-1})$ are known from the prior time-step $t=t_{i-1}$, then the constants A_i and B_i can be determined using Equations (18) and (19):

$$A_i = x_2(t_{i-1}) - a_1 Q_{1i} \quad (20)$$

$$B_i = x_3(t_{i-1}) - a_1 Q_{2i} \quad (21)$$

Then from Equations (18)-(21), the complete estimates for $x_2(t_i)$ and $x_3(t_i)$ with sampling time interval $h=t_i-t_{i-1}$ are obtained iteratively given $x_2(0)$ and $x_3(0)$ to start:

$$x_2(t_i) = x_2(t_{i-1})e^{-h/a_1} + a_1(1-e^{-h/a_1})Q_{1i} \quad (22)$$

$$x_3(t_i) = x_3(t_{i-1})e^{-h/a_1} + a_1(1-e^{-h/a_1})Q_{2i} \quad (23)$$

Using Equations (1)-(4), the equations for the full system at $t=t_i$ can be expressed as:

$$f_{1i}(\boldsymbol{\theta}) = m_1(\ddot{x}_1(t_i) + \ddot{x}_g(t_i)) + C_{11}\dot{x}_1(t_i) - C_{12}\dot{x}_2(t_i) + (K_1+K_2)x_1(t_i) - K_2 x_2(t_i) = 0 \quad (24)$$

$$f_{2i}(\boldsymbol{\theta}) = m_2(\ddot{x}_2(t_i) + \ddot{x}_g(t_i)) - C_{21}\dot{x}_1(t_i) + C_{22}\dot{x}_2(t_i) - C_{23}\dot{x}_3(t_i) - K_2 x_1(t_i) + (K_2+K_3)x_2(t_i) - K_3 x_3(t_i) = 0 \quad (25)$$

$$f_{3i}(\boldsymbol{\theta}) = m_3(\ddot{x}_3(t_i) + \ddot{x}_g(t_i)) - C_{32}\dot{x}_2(t_i) + C_{33}\dot{x}_3(t_i) - C_{34}\dot{x}_4(t_i) - K_3 x_2(t_i) + (K_3+K_4)x_3(t_i) - K_4 x_4(t_i) = 0 \quad (26)$$

$$f_{4i}(\boldsymbol{\theta}) = m_4(\ddot{x}_4(t_i) + \ddot{x}_g(t_i)) - C_{43}\dot{x}_3(t_i) + C_{44}\dot{x}_4(t_i) - K_4 x_3(t_i) + K_4 x_4(t_i) = 0 \quad (27)$$

where $\boldsymbol{\theta}= [K_1, K_2, K_3, K_4, a_0, a_1]$ is the parameter vector to be identified and it is iteratively updated using a Gauss-Newton formula:

$$\hat{\boldsymbol{\theta}}^{(s+1)} = \hat{\boldsymbol{\theta}}^{(s)} - \alpha(\mathbf{J}^{\mathbf{T}}\mathbf{J})^{-1}\mathbf{J}^{\mathbf{T}}\mathbf{R}^{(s)} \quad (28)$$

where s is the iteration step, α is the step length and $\mathbf{J}$ is the Jacobian matrix of $f_i(\hat{\boldsymbol{\theta}}^{(s)})$:

$$\mathbf{J} = [\mathbf{J}_1 \ \cdots \ \mathbf{J}_i \ \cdots \ \mathbf{J}_n]^{\mathbf{T}} \quad (29)$$

where $\mathbf{J}_i$ is determined as:

$$\mathbf{J}_i = \begin{bmatrix} \frac{\partial f_{1i}(\hat{\boldsymbol{\theta}}^{(s)})}{\partial K_1} & \frac{\partial f_{2i}(\hat{\boldsymbol{\theta}}^{(s)})}{\partial K_1} & \frac{\partial f_{3i}(\hat{\boldsymbol{\theta}}^{(s)})}{\partial K_1} & \frac{\partial f_{4i}(\hat{\boldsymbol{\theta}}^{(s)})}{\partial K_1} \\ \frac{\partial f_{1i}(\hat{\boldsymbol{\theta}}^{(s)})}{\partial K_2} & \frac{\partial f_{2i}(\hat{\boldsymbol{\theta}}^{(s)})}{\partial K_2} & \frac{\partial f_{3i}(\hat{\boldsymbol{\theta}}^{(s)})}{\partial K_2} & \frac{\partial f_{4i}(\hat{\boldsymbol{\theta}}^{(s)})}{\partial K_2} \\ \frac{\partial f_{1i}(\hat{\boldsymbol{\theta}}^{(s)})}{\partial K_3} & \frac{\partial f_{2i}(\hat{\boldsymbol{\theta}}^{(s)})}{\partial K_3} & \frac{\partial f_{3i}(\hat{\boldsymbol{\theta}}^{(s)})}{\partial K_3} & \frac{\partial f_{4i}(\hat{\boldsymbol{\theta}}^{(s)})}{\partial K_3} \\ \frac{\partial f_{1i}(\hat{\boldsymbol{\theta}}^{(s)})}{\partial K_4} & \frac{\partial f_{2i}(\hat{\boldsymbol{\theta}}^{(s)})}{\partial K_4} & \frac{\partial f_{3i}(\hat{\boldsymbol{\theta}}^{(s)})}{\partial K_4} & \frac{\partial f_{4i}(\hat{\boldsymbol{\theta}}^{(s)})}{\partial K_4} \\ \frac{\partial f_{1i}(\hat{\boldsymbol{\theta}}^{(s)})}{\partial a_0} & \frac{\partial f_{2i}(\hat{\boldsymbol{\theta}}^{(s)})}{\partial a_0} & \frac{\partial f_{3i}(\hat{\boldsymbol{\theta}}^{(s)})}{\partial a_0} & \frac{\partial f_{4i}(\hat{\boldsymbol{\theta}}^{(s)})}{\partial a_0} \\ \frac{\partial f_{1i}(\hat{\boldsymbol{\theta}}^{(s)})}{\partial a_1} & \frac{\partial f_{2i}(\hat{\boldsymbol{\theta}}^{(s)})}{\partial a_1} & \frac{\partial f_{3i}(\hat{\boldsymbol{\theta}}^{(s)})}{\partial a_1} & \frac{\partial f_{4i}(\hat{\boldsymbol{\theta}}^{(s)})}{\partial a_1} \end{bmatrix}^{\mathbf{T}} \quad (30)$$

where n is the number of time step samples. The error matrix $\mathbf{R}^{(s)}$ at iteration s is defined as:

$$\mathbf{R}^{(s)} = [f_{11}(\hat{\boldsymbol{\theta}}^{(s)}) \cdots \ f_{41}(\hat{\boldsymbol{\theta}}^{(s)}) \cdots \ f_{1i}(\hat{\boldsymbol{\theta}}^{(s)}) \cdots \ f_{4i}(\hat{\boldsymbol{\theta}}^{(s)}) \ \cdots f_{1n}(\hat{\boldsymbol{\theta}}^{(s)}) \ \cdots \ f_{4n}(\hat{\boldsymbol{\theta}}^{(s)})]^{\mathbf{T}} \quad (31)$$

The estimated $\hat{\boldsymbol{\theta}}$ seeks to minimize the error function:

$$\varepsilon(\hat{\boldsymbol{\theta}}) = \sum_{i=1}^{n} f_1(\hat{\boldsymbol{\theta}}) + \sum_{i=1}^{n} f_2(\hat{\boldsymbol{\theta}}) + \sum_{i=1}^{n} f_3(\hat{\boldsymbol{\theta}}) + \sum_{i=1}^{n} f_4(\hat{\boldsymbol{\theta}}) \quad (32)$$

SIMULATION AND VALIDATION CASE STUDY

A numerical study is first carried out to validate the performance of the proposed identification procedure in a controlled example where everything is known. The example structure was a four degree of freedom system with a set of parameters, including mass: m_1=3892e+3kg, m_2=12974e+3kg, m_3=2595e+3kg, m_4=3892e+3kg, and stiffness: K_1=728kN/mm, K_2=1120kN/mm, K_3=280kN/mm, K_4=300kN/mm. The Rayleigh damping coefficients are a_0=0.261 and a_1=0.0087, yielding damping ratios of 5% for the first and second modes.

The simulated structure was subjected to the El Centro earthquake, 1940. The system response was simulated using a Runge-Kutta method with a time step of Δt=0.005s. The calculated response data was utilised without added noise first, for proof of concept of the identification procedure. Figure 3 shows the estimates and convergence for the proposed parameters with different initial value guesses for $K_{1\text{-}4}$ and $a_{0\text{-}1}$. It can be seen that the final values of estimated parameters $K_{1\text{-}4}$ and a_1 converge to the exact values fast with different guesses. However, the convergence rate of a_0 is shown to be slower than a_1 because the proportion of the mass damping a_0 is very small and sometimes almost negligible for the construction of the classical damping matrix [15]. Thus, the weight of a_0 is much smaller than the weight of a_1 in the iteration process, which requires more iterations to obtain the exact value of a_0. However, they can all converge to the exact values with sufficiently small step size and large number of iterations. Thus, the identification method can yield accurate estimates of equivalent stiffness and damping coefficients of the system with clean measurements.

Figure 4 compares the estimated and true simulated responses for x_2 and x_3 using an initial guess of 200% of the exact structural parameter values. The estimated response fits well with the simulated response, indicating the method can yield good estimates of the unrecorded response for x_2 and x_3 with clean (noise-free) measurements of $\ddot{x}_1$ and $\ddot{x}_4$.

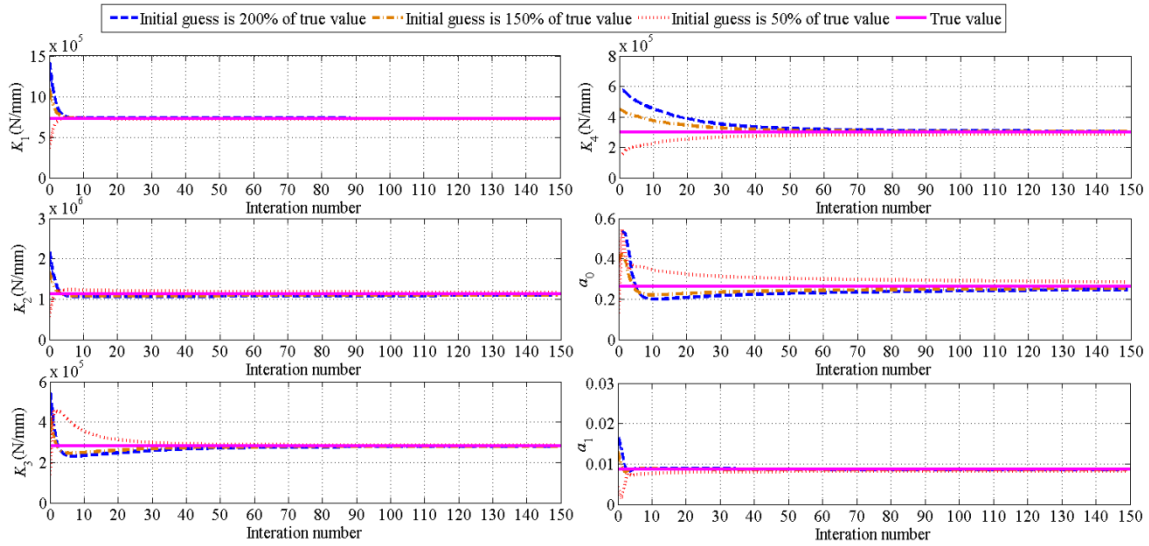

Figure 3: Parameter estimation performance with different initial guess values.

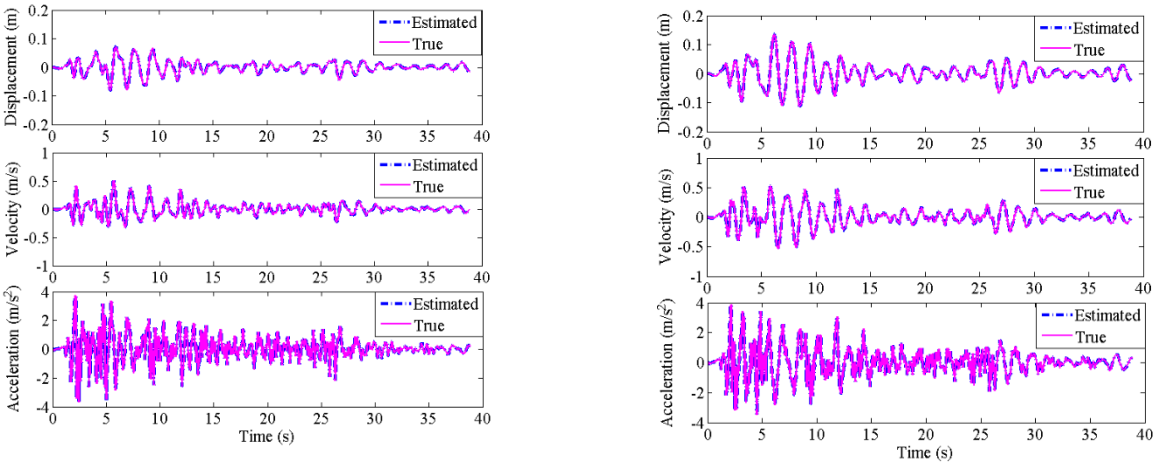

(a) (b)

Figure 4: Comparison of the estimated response and the true response for the unmeasured DOF using initial guess of 200% of exact parameter values: (a) the 2nd DOF; (b) the 3rd DOF.

To assess robustness to noise, a 10% random RMS noise was added to the measured ground and structural accelerations. The RMS noise is a random normal distribution with 99.7% of random values within 10% of the square root of the average of the clean (no noise) simulated measurement. The mean values of the estimated parameters for 100 Monte-Carlo runs with random added noise and different initial guesses, are shown in Table 3. It can be seen that the average error of estimated stiffness values is 16.6% with the largest Monte-Carlo mean error 31.7% using an initial guess of 200% of the exact parameter values. However, the average error of estimated stiffness values is 8.7% with the largest Monte-Carlo mean error 13.9% using initial guess of 150% of exact parameter values and 11.5% with the largest Monte-Carlo mean error 19.3% using an initial guess of 50% of exact parameter values.

In addition, the robustness to noise was also evaluated using different level noise with different initial guesses, as shown in Figure 5. It can be seen that the average errors show a small increase with increasing noise. Good estimates with average errors less than 10% were obtained using an initial guess of 150% of the exact parameter value for variable noise level. Thus, the initial guess affects identification accuracy with measurement noise. However, the estimated response using the estimated parameters shows good agreement with the true response for the unrecorded DOF, even with 10% added noise using an initial guess of 200% of exact parameters values, as shown in Figure 6.

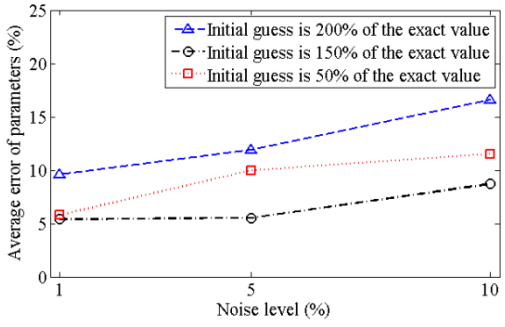

Figure 5: Average errors of the estimated parameters with variable noise level.

Table 3: Mean estimated results with 10% RMS noise for different initial guesses.

Parameters	K_1 (kN/mm)	K_2 (kN/mm)	K_3 (kN/mm)	K_4 (kN/mm)	a_0	a_1
Initial guess (200% of true value)	1456	2240	560	600	0.522	0.0174
Estimated	738	1053	231	395	0.336	0.0093
True	728	1120	280	300	0.261	0.0087
Monte-Carlo mean absolute error	1.4%	6.0%	17.5%	31.7%	28.7%	6.9%
Average error of parameters			16.6%			
Initial guess (150% of true value)	1092	1680	420	450	0.392	0.0131
Estimated	734	1074	241	340	0.296	0.0091
True	728	1120	280	300	0.261	0.0087
Monte-Carlo mean absolute error	0.8%	4.1%	13.9%	13.3%	13.4%	4.7%
Average error of parameters			8.7%			
Initial guess (50% of true value)	364	560	140	150	0.131	0.0044
Estimated	670	1132	301	242	0.212	0.0093
True	728	1120	280	300	0.261	0.0087
Monte-Carlo mean absolute error	8.0%	1.1%	7.5%	19.3%	18.8%	6.9%
Average error of parameters			11.5%			

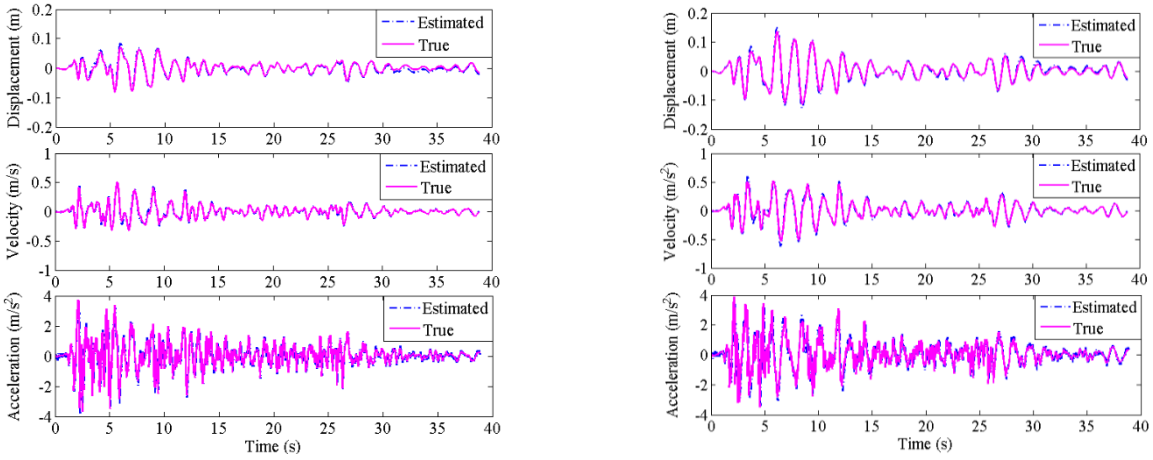

(a) (b)

Figure 6: Comparison of the estimated response and the true response for the unmeasured DOF with 10% RMS added noise using initial guess of 200% of exact parameter values: (a) the 2nd DOF; (b) the 3rd DOF.

IDENTIFICATION OF CWH BUILDING

The initial choice of the stiffness parameters for the superstructure is based on the assumption that the floors are rigid, the columns are axially inextensible and no additional stiffness is taken into account due to the non-structural walls and panels [15]. Torsion was neglected because recorded acceleration data from the northeast corner are very similar to the southwest corner, despite a slightly irregular cross section [4]. Therefore, stiffness, k_s, for each level without V-bracing is approximated using the sum of the lateral stiffness of all columns.

Considering approximately 80%-90% of the original elastic stiffness to be provided by the bracing [16], the stiffness for the lower floors with V-bracing was assumed to be two times k_s in the initial guess. The total seismic weight of the CWH building is approximately 170,000kN (17.3×10^6kg), including the dead loads and the live loads. In particular, the dead loads are calculated from the dimensions of the structural elements and a normal concrete density of 23kN/m^3 [17]. The basic live loads are taken as 2kN/m^2 for the lower seven levels with wards, and 3kN/m^2 for the top two levels with heavy equipment and utility [18]. In addition, the inner foundation and base isolation system are considered to be 10 percent of the seismic weight [19]. Thus, the estimated mass for each DOF is $m_1=2.6\times10^6$kg, $m_2=7.8\times10^6$kg, $m_3=3.9\times10^6$kg and $m_4=4.7\times10^6$kg.

The preliminary report shows that the post-yielding stiffness is not observed to be as prevalent as that of the pre-yielding stiffness from the measured force-to-deformation relationship, which indicate the isolation deformation that occurred is in the linear region of the isolators. Thus, the initial estimation of stiffness can be simply achieved by matching the slope of the measured response of the isolator and the initial stiffness of the base isolation system is then determined to be 1921kN/mm [19]. The classic Rayleigh damping ratio is assumed to be 5%

for the first mode, and higher damping is assumed for higher modes [20].

First Cross Validation

The method was first applied to identify the CWH building using the recorded accelerations of M_w6.0 earthquake. Although the overall duration of the earthquake excitation was ~ 232s, the parameter identification was carried out using only the main excitation measurements from 30s to 60s, as shown in Figure 7. The identified results were then used to simulate the response to the M_w5.8 earthquake.

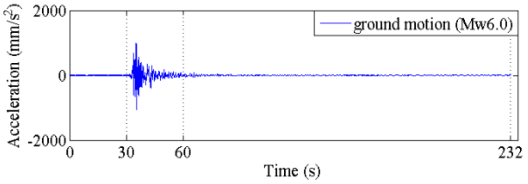

Figure 7: Recorded time history of ground acceleration for 6.0 magnitude earthquake.

Table 4 shows the assumed initial guess and final identified parameter values for the CWH building. The parameters T_1 and ζ_1 represent the fundamental natural period and damping factor. Comparisons of the estimated model and recorded accelerations at the first and fourth DOF, for both earthquakes are shown in Figure 8.

It can be seen that the assumed 4-DOF model was able to yield an accurate replication of the recorded accelerations from 42s to 60s for both events. However, the assumption of the superstructure as three DOFs system only allow for three natural modes included in the response analysis, which lead to a less consistent match between the estimated and recorded accelerations from 32s to 42s when higher modes and greater deformation of the structure occurred during the strong shock of the earthquake. Thus, the flexibility of the CWH building was not as exactly modelled using the four DOF model and a model with increased DOFs would produce a better replication of the actual response if more stories were instrumented for the CWH building during the earthquakes.

However, it can be seen from Table 5 that the differences between the recorded and estimated peak acceleration are a maximum of 5.6% and 14.1% for the first and fourth DOF, respectively. In addition, Table 5 shows the results of the cross correlation coefficients ($R_{corrcoef}$) and the mean absolute percentage errors (MAPE) between the estimated model and recorded acceleration response to evaluate the accuracy of the identified model time histories [21] ($R_{corrcoef}$ and MAPE were calculated:

$$\bar{X}_{actual} = \sqrt{\left(\sum_{i=1}^{N} X_{i,actual}^2 - \frac{\left(\sum_{i=1}^{N} X_{i,actual} \right)^2}{N} \right)} \tag{33}$$

$$\bar{X}_{estimated} = \sqrt{\left(\sum_{i=1}^{N} X_{i,estimated}^2 - \frac{\left(\sum_{i=1}^{N} X_{i,estimated} \right)^2}{N} \right)} \tag{34}$$

$$R_{corrcoef} = \frac{\sum_{i=1}^{N} X_{i,actual} X_{i,estimated} - \frac{\sum_{i=1}^{N} X_{i,actual} \sum_{i=1}^{N} X_{i,estimated}}{N}}{\bar{X}_{actual} \cdot \bar{X}_{estimated}} \tag{35}$$

$$MAPE = \frac{\sum_{i=1}^{N} \left| X_{i,actual} - X_{i,estimated} \right|}{\sum_{i=1}^{N} \left| X_{i,actual} \right|} \times 100\% \tag{36}$$

where X_{actual} is the recorded accelerations, $X_{estimated}$ is the estimated model accelerations, and N is the number of estimated data points. From Table 5, it can be seen that the values of MAPE for the M_w6.0 earthquake are small with the largest value 5.1% and the values of MAPE for the M_w5.8 event is relatively larger with the largest value 13.7%. However, the values of $R_{corrcoef}$ are more than 0.74 for both events, which indicates a strong positive correlation between the estimated and recorded measurements.

Table 4: Identified results for CWH building using the data of M_w6.0.

Parameters	K_1 (kN/mm)	K_1 (kN/mm)	K_1 (kN/mm)	K_1 (kN/mm)	a_0	a_1	T_1 (s)	ζ_1
Initial guess	1921	1120	300	400	0.269	0.0088	1.42	5%
Estimated (E6.0)	1594	1261	336	458	0.661	0.0090	1.37	9%

Table 5: Results of peak acceleration, $R_{corrcoef}$ and MAPE using E6.0.

Identified parameters	Earthquake		Peak acceleration (kN/mm)			$R_{corrcoef}$	MAPE
			Recorded	Estimated	Error		
E6.0	M_w 6.0	1st DOF	1201	1268	5.6%	0.80	5.1%
		4th DOF	1742	1805	3.6%	0.76	3.9%
	M_w 5.8	1st DOF	771	778	1.0%	0.74	13.7%
		4th DOF	1536	1753	14.1%	0.78	5.3%

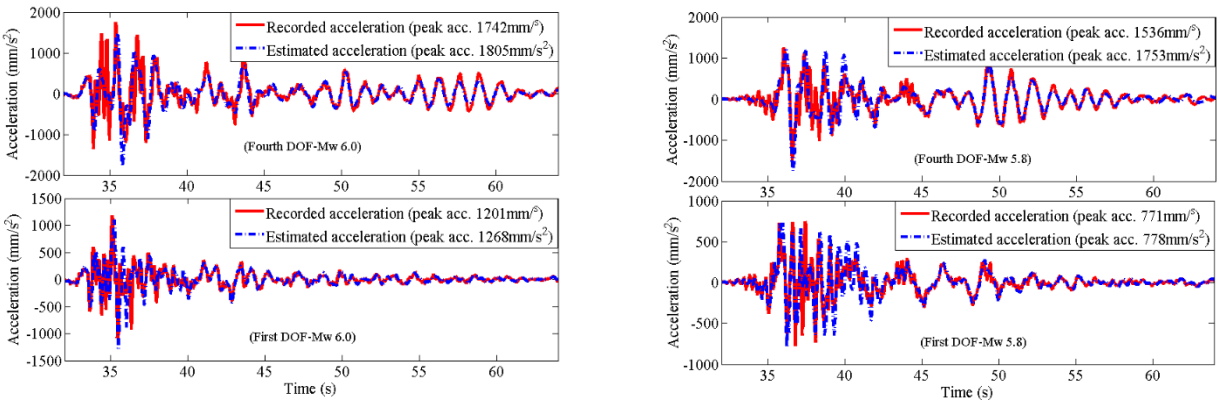

(a) (b)

Figure 8: Comparison of estimated model and the recorded accelerations: (a) M_w 6.0 earthquake; (b) M_w 5.8 earthquake.

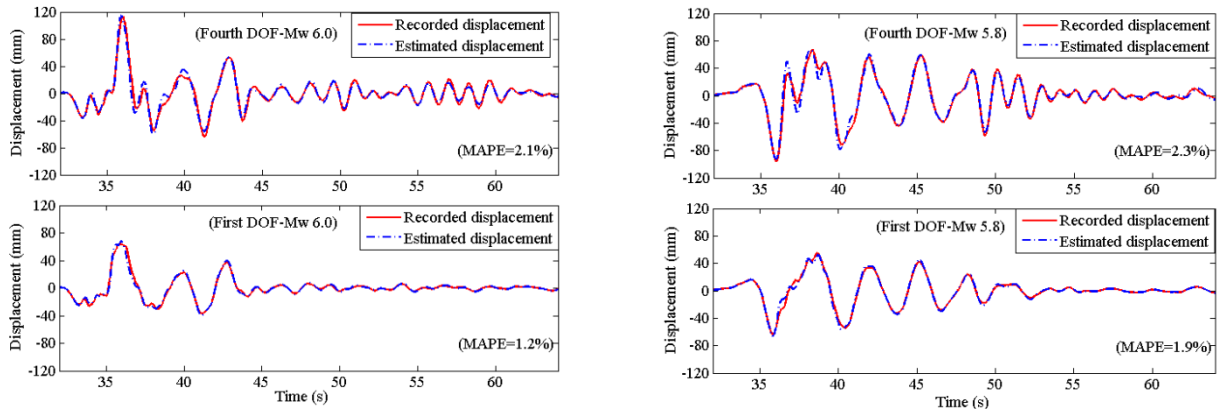

(a) (b)

Figure 9: Comparison of estimated and the recorded displacements: (a) M_w 6.0 earthquake; (b) M_w 5.8 earthquake.

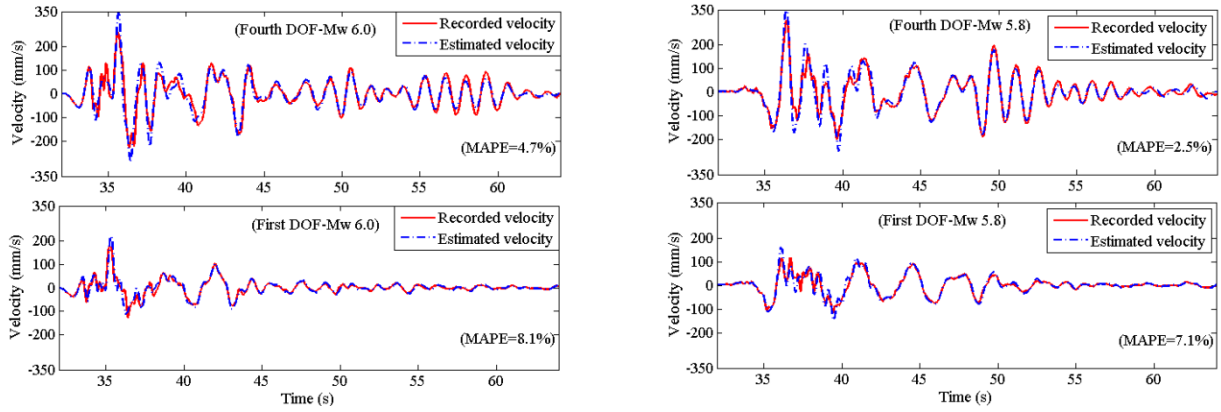

(a) (b)

Figure 10: Comparison of estimated and the recorded velocities: (a) M_w 6.0 earthquake; (b) M_w 5.8 earthquake.

In addition, the recorded velocities and displacements computed by single and double integration of measured accelerations are compared to the model estimated results, as shown in Figures 9 and 10. It can be seen that the peak values of the estimated displacement and velocity are slightly larger than the recorded values. However, the phase of the time histories matched well between the estimated and recorded response.

These results indicate that the identified shear type linear model can be considered to be sufficient for the prediction of the structural response during these two events. The CWH building performed elastically with no significant stiffness loss during these two events because the seismic response for both events can be predicted well using the identified parameters from the M_w 6.0 event (E6.0).

Second Cross Validation

The M_w5.8 recorded data was also used to identify the parameters as shown in Table 6, and the identified parameters were then used to simulate the response to the M_w6.0 earthquake. This approach reverses the analysis of M_w6.0 to further assess the robustness of this identification method. Table 7 shows the results of the comparison of peak accelerations between the recorded and estimated response, and the calculated $R_{corrcoef}$ and MAPE.

It can be seen from Table 6 that the identified parameters E5.8 using the data of M_w5.8 are slightly different from the identified parameters E6.0 using the data from the M_w6.0 event. This discrepancy could be caused by the effect of the adjacent Christchurch Hospital building with interconnecting walkways at the bottom 4 floors, and the soil-structure interaction [12]. However, the difference of peak accelerations between the recorded and estimated response are less than 4.7% for M_w5.8 earthquake and 12.5% for M_w6.0 earthquake, respectively. The values of MAPE are less than 10.9% for both events. In addition, the values of $R_{corrcoef}$ are more than 0.76 for M_w5.8 earthquake and 0.73 for M_w6.0 earthquake, respectively. Thus, given very similar results to the prior, reversed analysis, the identified parameters E5.8 also well predict the seismic response for both events and yield slightly better estimated model responses.

Table 6: Identified results for CWH building using the data of M_w5.8.

Parameters	K_1 (kN/mm)	K_1 (kN/mm)	K_1 (kN/mm)	K_1 (kN/mm)	a_0	a_1	T_1 (s)	ζ_1
Initial guess	1921	1120	300	400	0.269	0.0088	1.42	5%
Estimated (E5.8)	1633	1043	305	395	0.607	0.0171	1.45	10%

Table 7: Results of peak acceleration, $R_{corrcoef}$ and MAPE using E5.8.

Identified parameters	Earthquake		Peak acceleration (kN/mm)			$R_{corrcoef}$	MAPE
			Recorded	Estimated	Error		
E5.8	M_w 6.0	1st DOF	1201	1050	12.5%	0.82	4.0%
		4th DOF	1742	1528	12.2%	0.73	8.1%
	M_w 5.8	1st DOF	771	735	4.7%	0.84	4.2%
		4th DOF	1536	1505	2.0%	0.76	10.9%

.

CONCLUSION

This research identifies stiffness and Rayleigh damping coefficients of the base isolated CWH building using a modified Gauss-Newton method and the recorded response of two large earthquakes in Christchurch that occurred within a few hours in December 2011. Numerical validation of the identification method showed that estimated structural stiffness and damping coefficients converge from a range of initial guesses and are robust to added noise. Two unique cross validation identification analyses of the CWH building showed that using identified parameters from provided a very good match of model and measured response for the other large event, validating the chosen model. Thus, the comparison of measured and identified model response also show that the structure behaved essentially linearly in both events, regardless of the event used to identify the model, and that the base isolation system acted in the stiff linear range, all of which matches other preliminary reports. These thus provide good estimates of the structural properties for any subsequent response modelling of the structure.

ACKNOWLEDGMENTS

The authors acknowledge the China Scholarship Council (No. 201306260119) in support of this study.

REFERENCES

1 Nagarajaiah S and Sun X (2000). "Response of Base-Isolated Usc Hospital Building in Northridge Earthquake". *Journal of Structural Engineering*, **126**(10):1177-1186.

2 Miwada G, Yoshida O, Ishikawa R and Nakamura M (2012). "Observation Records of Base-Isolated Buildings in Strong Motion Area During the 2011 Off the Pacific Coast of Tohuku Earthquake". *Proceedings of the International Symposium on Engineering Lessons Learned from the 2011 Great East Japan Earthquake*, Tokyo, Japan, March 1-4, 1017-1024.

3 Hijikata K, Takahashi M, Aoyagi T and Mashimo M (2011). "Behavior of a Base Isolated Building at Fukushima Dai-Ichi Nuclear Power Plant During the Great East Japan Earthquake". *Proceedings of the International Symposium on Engineering Lessons Learned from the*

2011 Great East Japan Earthquake, Tokyo, Japan, March 1-4, 1542-1551.

4 Sridhar A, Kuang A, Garven J, Gutschmidt S, Chase JG, Gavin HP, Nigbor RL, Rodgers GW and MacRae GA (2014). "Christchurch Women's Hospital: Analysis of Measured Earthquake Data During the 2011-2012 Christchurch Earthquakes". *Earthquake Spectra*, **30**(1):383-400.

5 Stewart JP, Conte JP and Aiken ID (1999). "Observed Behavior of Seismically Isolated Buildings". *Journal of Structural Engineering*, **125**(9):955-964.

6 Furukawa T, Ito M, Izawa K and Noori MN (2005). "System Identification of Base-Isolated Building Using Seismic Response Data". *Journal of Engineering Mechanics*, **131**(3):268-275.

7 Huang M-C, Wang Y-P, Chang J-R and Chen Y-H (2009). "Physical-Parameter Identification of Base-Isolated Buildings Using Backbone Curves". *Journal of Sructural Engineering*, **135**(9):1107-1114.

8 Xu C, Chase JG and Rodgers GW (2014). "Physical Parameter Identification of Nonlinear Base-Isolated Buildings Using Seismic Response Data". *Computers & Structures*, **145**(1):47-57.

9 Kulkarni JA and Jangid R (2002). "Rigid Body Response of Base - Isolated Structures". *Journal of Structural Control*, **9**(3):171-188.

10 Kulkarni JA and Jangid R (2003). "Effects of Superstructure Flexibility on the Response of Base-Isolated Structures". *Shock and Vibration*, **10**(1):1-13.

11 Park Y, Wen Y and Ang A (1986). "Random Vibration of Hysteretic Systems under Bi - Directional Ground Motions". *Earthquake Engineering & Structural Dynamics*, **14**(4): 543-557.

12 Gavin HP and Wilkinson G (2010). "Preliminary Observations of the Effects of the 2010 Darfield Earthquake on the Base-Isolated Christchurch Women's Hospital". *Bulletin of the New Zealand Society for Earthquake Engineering*, **43**(4):360-367.

13 Matsagar VA and Jangid R (2008). "Base Isolation for Seismic Retrofitting of Structures". *Practice Periodical on Structural Design and Construction*, **13**(4):175-185.

14 Chen J, Liu W, Peng Y and Li J (2007). "Stochastic Seismic Response and Reliability Analysis of Base-Isolated Structures". *Journal of Earthquake Engineering*, **11**(6):903-924.

15 Chopra AK (1995). "*Dynamics of Structures*". Prentice Hall, New Jersey, 794pp.

16 Sabelli R, Roeder CW and Hajjar JF (2013). "*Seismic Design of Steel Special Concentrically Braced Frame Systems*". NIST GCR 13-917-24, National Institute of Standards and Technology, California, 36pp.

17 Cement & Concrete Association of New Zealand (2010). "*New Zealand Guide to Concrete Construction*". Cement & Concrete Association of New Zealand (CCANZ), Wellington, 246pp.

18 Standards New Zealand (1992). "*Code of Practice for General Structural Design and Design Loadings for Buildings*". Standards New Zealand, Wellington, 134pp.

19 Kuang A, Sridhar A, Garven J, Gutschmidt S, Rodgers GW, Chase JG, Gavin HP, Nigbor R and Macrae G (2014). "*Christchurch Women's Hosptial: Performance Analysis of the Base-Isolation System During the Series of Canterbury Earthquakes 2010-2011*". 2014.5.5, Univeristy of Canterbury, Christchurch, 37pp.

20 Clough RW and Penzien J (1993). "*Dynamics of Structures*". McGraw-Hill, New York, 768pp.

21 Swanson DA, Tayman J and Bryan T (2011). "Mape-R: A Rescaled Measure of Accuracy for Cross-Sectional Subnational Population Forecasts". *Journal of Population Research*, **28**(2-3):225-243.